Kondo effect in a topological insulator quantum dot

Xianhao Xin and Di Zhou

Kondo effect in a topological insulator quantum dot

Xianhao Xin and Di Zhou

Department of Physics, University of Illinois at Urbana-Champaign,
1110 W. Green St. , Urbana, IL 61801-3080, USA

We investigate the non-equilibrium transport properties of a topological insulator quantum dot (TIQD) in the Coulomb blockade and Kondo regime theoretically. An Anderson impurity model is applied to a TIQD system coupled to two external leads, and we show that the model realizes the spin-orbital Kondo effect at Dirac point where the edge states are not split by a finite-size effect, leading to an additional $SU(4)$ symmetry because of the presence of strong mixture among four internal degrees of freedom. In a more realistic situation where the degeneracy is lifted due to the finite-size effect, we demonstrate that there is a richer structure in transport measurements. We illustrate a continuous crossover from four (spin and orbital) Coulomb peaks with large inter-pair spacing and small intra-pair spacing to a double-peak structure in the local density of states (LDOS) as increasing the hybridization strength Γ within the Coulomb blockade regime. When temperature falls below the Kondo temperature T_K, four Kondo peaks show up in the non-equilibrium LDOS. Two of them are located at the chemical potential of each lead, and the other two are shift away from the chemical potential by the amount proportional to the TIQD's bare energy level, leading to a triple-peak structure in the differential conductance when a bias voltage is applied.

I. INTRODUCTION

The study of transport properties in quantum dot (QD) systems is one of the fundamental paradigms of mesoscopic condensed matter physics. Compared to conventional condensed matter systems, the QD provides a controllable circumstance to investigate the strong correlated physics such as Kondo effect. The conventional Kondo effect requires the presence of a magnetic impurity in the bulk of material. However the localized electron within a QD behaves like a quantum impurity with spin 1/2. It enables many studies of Kondo effect in QD systems. At low temperatures, a spin singlet state is formed between the localized electrons in a QD and the conduction electrons from external leads at the Fermi level. Hence QD systems exhibit the Kondo effect at the temperatures below the Kondo temperature T_K.[1] The spin of localized electrons is strongly correlated with conduction electrons and are screened accordingly. The competition between Coulomb interaction and band hybridization plays an important role to produce the Kondo effect. The Anderson's impurity model provides an excellent description of Kondo physics at low temperatures.[2] One of the most remarkable features of Kondo effect is the emergence of a Kondo resonance at the Fermi level in the LDOS. As a result, the theory predicts a zero-bias peak in the differential conductance.[3,4] Kondo effect and its related transport properties have been observed experimentally in many QD systems.[5–9]

Recent development in nano-fabrication techniques allows controllable studies of Kondo physics in more complex coupled QD systems as well as carbon nanotube quantum dot (CNQD) systems. For double quantum dot (DQD) devices, spin degrees of freedom within each dot and orbital degrees of freedom crossing two dots are coupled each other, leading to a realization of so-called spin-orbital Kondo effect. The orbital degrees of freedom in DQDs play the role of psuedospin in addition to the spin degrees of freedom. Similarly, the orbital degrees of freedom in CNQD systems correspond to the clockwise and counterclockwise wrapping modes in CNQDs. It is the quantum fluctuations among QD's four internal degrees of freedom that result in the spin-orbital Kondo effect. The spin-orbital Kondo effect has been investigated in great amount in CNQDs,[10–25] vertical quantum dots,[26] grain-dot systems,[27,28] and parallel quantum dots.[29–43] Compared with the conventional Kondo effect, in which only spin degrees of freedom are involved, the spin-orbital Kondo effect is characterized by the intra-dot and inter-dot interactions in DQD systems. The intra-dot interaction is determined by usual spin Kondo correlation, while the inter-dot interaction is associated with the on-site Coulomb interaction between two QDs. A $SU(4)$ Kondo state with entangled spin and orbital degrees of freedom emerges when intra-dot interaction is fine-tuned to be inter-dot interaction. One of the technical obstructions to observe the $SU(4)$ spin-orbital Kondo effect in DQD systems is because of the difficulty of fine-tuning intra- and inter-dot interactions symmetrically. These two on-site interactions are not directly measurable physical quantities within our knowledge. They can only be inferred through fitting experimental data to some theoretical formulas, thereby it makes the symmetrical control even worse experimentally. CNQD systems face the similar obstacles since there is no guarantee that the on-site Coulomb interactions between spin degrees of freedom should be identical to those between wrapping (orbital) modes. A fine-tuning among experimental parameters is required in order to realize the $SU(4)$ Kondo effect in DQD systems as well as CNQD systems.

Because of the requirement of fine-tuning in DQD systems as well as CNQD systems, we propose another way

to realize the spin-orbit Kondo effect based on one QD made by a topological insulator (TI). TIs have nontrivial bulk band topology with the presence of peculiar metallic states on their surfaces. These surface states are protected by time-reversal symmetry, hence are stable against any time-reversal invariant perturbation. The back scattering, which requires an electron to flip its spin, is strictly prohibited due to the presence of time-reversal symmetry. Gapless surface states can be described by a massless Dirac equation, where spin and momentum are locked together.[44–48] The electrical conductance due to time-reversal symmetry protected edge states was measured in a quantum well structure of $HgTe/CdTe$, showing a signature of the existence of quantum spin Hall insulators (two dimensional TIs).[49] The experimental realizations of three dimensional TIs' symmetry protected surface states were also observed afterwards in materials such as Bi_2Se_3 and Bi_2Te_3 using angle-resolved photoemission spectroscopy (ARPES).[50–52] In addition, there are many other researches studying the quantum effect induced by magnetic impurities on the surface of TIs.[53–58] However the study of Kondo effect in TIQDs is still sparse. Because of the intrinsic spin-orbital locking feature existed in TI materials, a TIQD is a natural candidate to realize the spin-orbital Kondo effect. One of the advantages of using such devices is that it can avoid the possible fine-tuning between intra-dot and inter-dot Coulomb repulsive interactions as usually required by conventional DQD systems as well as CNQD systems. We highlight the fact that $SU(4)$ Kondo physics can be probed in such a setup, eliminating the obstacle faced by DQD and CNQD systems. Recent successful fabrication of the QD made by Bi_2Se_3 makes the study of the spin-orbital Kondo effect in TIQDs more promising in the future.[59]

This article is organized as follows. In Sec. II, we introduce the model starting from an Anderson-type Hamiltonian. We demonstrate that the effective Anderson Hamiltonian exhibits $SU(4)$ Kondo features at Dirac point due to strong entanglement between spin degrees of freedom and orbital degrees of freedom. In Sec. III, the LDOS based on the non-equilibrium Green's function method is calculated in the mean-field regime, Coulomb blockage regime, and Kondo regime respectively. In the Kondo regime, a triple-peak structure in the differential conductance is also shown in Sec. III. Main results are then summarized in Sec. IV. Some detailed calculations of the non-equilibrium Green's functions are presented in appendices.

II. MODEL HAMILTONIAN

We consider a QD formed in a thin circular TI slab as depicted schematically in Fig. 1. The dot is coupled to two external leads symmetrically. A gate voltage is applied to the system so that only the energy levels near Dirac point contribute to transport through the TIQD.
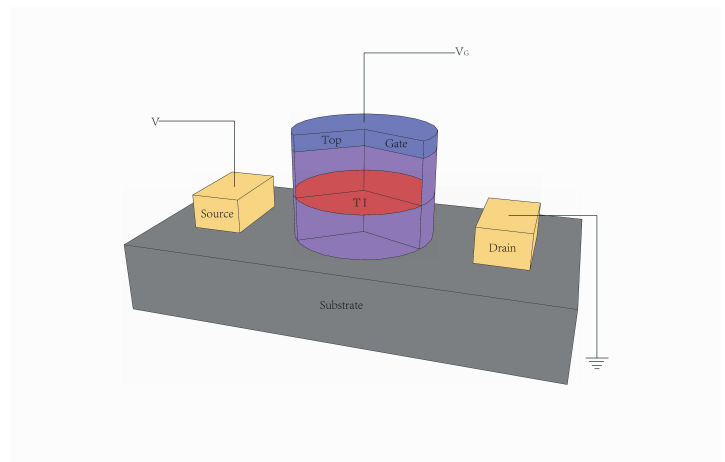

FIG. 1: Sketch of a TIQD attached to two external leads. The geometry of the TIQD is a thin circular slab. The gate voltage V_G adjusts the energy levels so that only those levels near Dirac point contribute to the transport properties of the TIQD. The biased voltage eV is controlled by the difference between left and right leads' chemical potential: $eV = \mu_L - \mu_R$.

A full model Hamiltonian can be written as

$$H = H_{dot} + H_{col} + H_l + H_t. \tag{1}$$

The first term, H_{dot}, describes the electrons' edge states in a TIQD. It has been shown that the edge states of a disk-shaped TIQD can be characterized as massless Dirac fermions.[60] These edge states are fully spin-polarized and exhibit so-called spin-angular momentum locking: spin-up electrons rotate clockwise, while spin-down electrons rotate counterclockwise. The similar conclusion can also be applied to a three-dimensional TIQD, where its surface states can be approximated by Dirac equations with spin connection.[61,62] Therefore the low energy spectrum of a circular shaped TIQD is linear against the angular momentum quantum number m, and the low energy edge states are described by a four-band effective Hamiltonian in basis $|\uparrow +\rangle$, $|\uparrow -\rangle$, $|\downarrow +\rangle$, and $|\downarrow -\rangle$. The effective Hamiltonian then reads

$$H_{dot} = \sum_{\substack{m, \\ \sigma=\uparrow,\downarrow, \\ \tau=+,-}} c^\dagger_{m,\sigma\tau} \mathscr{H}(m)_{\sigma\tau,\sigma'\tau'} c_{m,\sigma'\tau'},$$

where

$$\mathscr{H}(m) = \begin{pmatrix} A\hbar v_F k_F m \sigma_x & \Delta\mathbb{I} \\ \Delta^*\mathbb{I} & -A\hbar v_F k_F m \sigma_x \end{pmatrix}, \tag{2}$$

in which A is a dimensionless constant of order 1, v_F is the Fermi velocity, k_F is the Fermi wave-vector and m is the angular momentum quantum number.

Here $c^\dagger_{m,\sigma\tau}$ ($c_{m,\sigma\tau}$) creates (annihilates) a localized electron with angular momentum m and spin $\sigma = \{\uparrow,\downarrow\}$ on either top ($\tau = \{+\}$) or bottom ($\tau = \{-\}$) side of the TIQD. Δ is a finite size energy gap produced by the coupling between the top and bottom edge states. The geometry of the TIQD considered in this paper is a circular thin slab with thickness L. In this case, the level spacing of the edge states would be dominated by the size of the TI slab, while the finite size gap Δ decays in an exponential law of the thickness L.[63] It is the quantum fluctuations among four internal channels: $\{\uparrow +, \downarrow +, \uparrow -, \downarrow -\}$ that lead to an unusual strongly correlated Fermi liquid behavior.

Hamiltonian (2) can be diagonalized with eigenvalues $E_\pm = \pm\sqrt{A^2\hbar^2 v_F^2 k_F^2 m^2 + |\Delta|^2}$ by introducing a new set of basis states:

$$c_\alpha = \sum_{\sigma\tau} \mathscr{U}_{\alpha,\sigma\tau} c_{\sigma\tau}, \qquad \alpha = 1, 2, 3, 4; \qquad (3)$$

$$\sigma\tau = \uparrow+, \downarrow+, \uparrow-, \downarrow-,$$

where matrix $\mathscr{U}$ is defined as

$$\mathscr{U} = \frac{1}{\sqrt{2}} \begin{pmatrix} \sin\frac{\Omega}{2} & \cos\frac{\Omega}{2} & -e^{i\phi}\sin\frac{\Omega}{2} & e^{i\phi}\cos\frac{\Omega}{2} \\ \cos\frac{\Omega}{2} & \sin\frac{\Omega}{2} & e^{i\phi}\cos\frac{\Omega}{2} & -e^{i\phi}\sin\frac{\Omega}{2} \\ -\cos\frac{\Omega}{2} & \sin\frac{\Omega}{2} & e^{i\phi}\cos\frac{\Omega}{2} & e^{i\phi}\sin\frac{\Omega}{2} \\ \sin\frac{\Omega}{2} & -\cos\frac{\Omega}{2} & e^{i\phi}\sin\frac{\Omega}{2} & e^{i\phi}\cos\frac{\Omega}{2} \end{pmatrix}.$$

The parameters in matrix $\mathscr{U}$ are defined as $e^{i\phi} = \frac{\Delta}{|\Delta|}$, $\sin\Omega = \frac{A\hbar v_F k_F m}{E_+}$ and $\cos\Omega = \frac{|\Delta|}{E_+}$. Then Eq. (2) can be rewritten in terms of the new basis vectors $\{c_\alpha\}$s as

$$H_{dot} = \sum_m \sum_\alpha \epsilon_\alpha(m) c^\dagger_\alpha c_\alpha, \qquad (4)$$

where $\epsilon_1 = \epsilon_2 = E_+$ and $\epsilon_3 = \epsilon_4 = E_-$. We have to point out that Hamiltonian (4) has four-fold degeneracy at Dirac point when $\Delta = 0$. In practice, this four-fold degeneracy nearly retains even if $\Delta \neq 0$ provided Δ is much smaller than all other energy scales, such as temperature. This is an important aspect to realize the $SU(4)$ Kondo effect.

The second term, H_{col}, represents the on-site Coulomb repulsive interaction between the localized electrons in the TIQD. The strength of repulsive interaction is characterized by a Coulomb integral[2]

$$U_{\alpha\alpha'} = \int |\Psi_\alpha(\mathbf{r_1})|^2 e^2 |\mathbf{r_{12}}|^{-1} |\Psi_{\alpha'}(\mathbf{r_2})|^2 d\mathbf{r_1} d\mathbf{r_2}, \quad (5)$$

where $\Psi_\alpha \equiv c^\dagger_\alpha |0\rangle$ is the eigenfunction of Hamiltonian (2). The Coulomb repulsive interaction strength, $U_{\alpha\alpha'}$, is approximately proportional to the inverse of the slab's thickness L.

Furthermore, we notice that the density distributions of Ψ_α are related to the density distributions of edge states' wave-functions through the relations:

$$|\Psi_{1,4}|^2 = \frac{1}{2}\left(\sin^2\frac{\Omega}{2}\left(|\Psi_{\uparrow+}|^2 + |\Psi_{\uparrow-}|^2\right) + \cos^2\frac{\Omega}{2}\left(|\Psi_{\downarrow+}|^2 + |\Psi_{\downarrow-}|^2\right)\right)$$

$$|\Psi_{2,3}|^2 = \frac{1}{2}\left(\cos^2\frac{\Omega}{2}\left(|\Psi_{\uparrow+}|^2 + |\Psi_{\uparrow-}|^2\right) + \sin^2\frac{\Omega}{2}\left(|\Psi_{\downarrow+}|^2 + |\Psi_{\downarrow-}|^2\right)\right).$$

Since the top and bottom edge states' wave-functions $\Psi_{\downarrow\pm}$ are related by means of the time-reversal operation: $\Psi_{\downarrow\pm} = \Theta\Psi_{\uparrow\mp}$, we find that the density distributions of Ψ_α equally mix the density distributions of both top and bottom edge states:

$$|\Psi_\alpha|^2 = \frac{1}{2}|\Psi_+|^2 + \frac{1}{2}|\Psi_-|^2, \qquad \alpha = 1, 2, 3, 4, \qquad (6)$$

where $|\Psi_\pm|^2 \equiv |\Psi_{\uparrow\pm}|^2 = |\Psi_{\downarrow\pm}|^2$ because of the presence of time-reversal symmetry in the TIQD system. This implies that all four internal states must have the same Coulomb integrals: $U_{\alpha\alpha'} = U$. Formally, an exchange and correlation term can be written as

$$\frac{1}{2}U\left(\sum_\alpha n_\alpha\right)\left(\sum_\alpha n_\alpha\right) - \frac{1}{2}U\left(\sum_\alpha n_\alpha n_\alpha\right),$$

where $n_\alpha = c^\dagger_\alpha c_\alpha$ and we have subtracted the contribution due to self-correlation. Therefore H_{col} can be schematized as

$$H_{col} = U\sum_{\alpha<\alpha'} n_\alpha n_{\alpha'}, \qquad (7)$$

where the on-site Coulomb integral $U_{\alpha\alpha'}$ is independent of all internal degrees of freedom. This is the key to realize $SU(4)$ symmetry in the TIQD system without the requirement of fine-tuning. Moreover, we notice that Hamiltonian (7) is time-reversal invariant, thus the single-particle edge states remain intact even in the presence of large on-site Coulomb repulsive interactions.

The third term, H_l, describes the unperturbed states of conduction electrons from left or right reservoir:

$$H_l = \sum_{\substack{\tau=1,2 \\ \sigma=\uparrow,\downarrow}} \sum_{k \in L,R} \epsilon_k c^\dagger_{k,\tau,\sigma} c_{k,\tau,\sigma}, \qquad (8)$$

where ϵ_k is the energy spectrum of conduction electrons with momentum k, L/R represents left or right lead, and $c^\dagger_{k,\tau,\sigma}(c_{k,\tau,\sigma})$ creates (annihilates) a conduction electron with spin σ in channel τ. Without loss of generality, we assume that there are two distinguished groups of channels $\tau = 1, 2$ in left/right leads. Since the energy spectrum ϵ_k is independent of the spin index σ as well as the artificial orbital index τ, Eq. (8) remains diagonal after rotating the basis vectors within the spin-orbital σ-τ subspace. Therefore one can rewrite Eq. (8) in terms of a new set of basis states $\{|\alpha\rangle\}$s under the transformation (3) as

$$H_l = \sum_{\alpha,k \in L,R} \epsilon_k c^\dagger_{k\alpha} c_{k\alpha}. \qquad (9)$$

We make a further assumption that the conduction bands of both two external leads are flat with band width $2W$. The corresponding LDOS is then given by $\tilde{\rho}(\epsilon) = \tilde{\rho}_0 = 1/(2W)$. This assumption is made just for simplicity and can be easily released. One can verify that

a reasonable energy variation of $\tilde{\rho}(\epsilon)$ does not change the results qualitatively.

The fourth part of Eq. (1) is a hybridization term, which is described as

$$H_t = \sum_{\alpha, k \in L, R} \left(V_{k\alpha} c_\alpha^\dagger c_{k\alpha} + H.c. \right). \tag{10}$$

Thus we conclude that the model Hamiltonian describing a TIQD coupled to two external leads can be written as

$$H = \sum_{\alpha, k \in L, R} \epsilon_k c_{k\alpha}^\dagger c_{k\alpha} + \sum_m \sum_\alpha \epsilon_\alpha(m) c_\alpha^\dagger c_\alpha \tag{11}$$

$$+ U \sum_{\alpha < \alpha'} n_\alpha n_{\alpha'} + \sum_{\alpha, k \in L, R} \left(V_{k\alpha} c_\alpha^\dagger c_{k\alpha} + H.c. \right).$$

Since we are only interested in the temperature scales that are much smaller than the average level spacing of a TIQD, we consider the case that the angular momentum quantum number m takes only one single value in the second term of Eq. (11). The method we discuss in this paper can be readily extended to multiple-m value cases. We conclude that full Hamiltonian (11) realizes the spin-orbital Kondo effect because of the existence of strong mixing among the TIQD's four internal channels. The spin-orbital Kondo effect in the TIQD system is characterized by a constant Coulomb repulsive interaction strength U. In an idealized situation where all four internal states are energetically degenerate at Dirac point, the TIQD exhibits an additional $SU(4)$ symmetry and the spin-orbital Kondo effect emerges. On the other hand, in general, the four-fold degeneracy can be lifted by a finite size effect, leading to a triple-peak structure in the differential conductance within the Kondo regime as shown in the following.

III. NON-EQUILIBRIUM GREEN'S FUNCTION METHOD

We consider a problem involving a TIQD coupled to two external leads. A non-equilibrium Green's function is constructed through the equations-of-motion (EOM) method.[4,64,65] In the Heisenberg representation, the time-evolution of a Heisenberg operator is determined by its commutator with the corresponding Hamiltonian. This is the essence of the EOM method. Two coupled equations describing the equations of motion governed by Hamiltonian (11) are obtained as

$$i\hbar \frac{\partial}{\partial t} c_\alpha = \epsilon_\alpha c_\alpha + \sum_{k \in L, R} V_{k\alpha} c_{k\alpha} + \sum_{\alpha' \neq \alpha} U c_{\alpha'}^\dagger c_{\alpha'} c_\alpha,$$

$$i\hbar \frac{\partial}{\partial t} c_{k\alpha} = (\epsilon_k - i\eta) c_{k\alpha} + V_{k\alpha}^* c_\alpha + S_{k\alpha}, \tag{12}$$

where a source term $S_{k\alpha}$ is added into the second term of Eqs. (12) ad hoc. The solution of the second equation

in Eqs. (12) reads

$$c_{k\alpha} = c_{k\alpha}^{(0)} + \int_{-\infty}^{+\infty} dt' V_{k\alpha}^* G_{k\alpha}(t - t') c_\alpha(t'), \tag{13}$$

where $G_{k\alpha}(t - t') = \frac{1}{i\hbar} \theta(t - t') e^{-\frac{i}{\hbar}(\epsilon_k - i\eta)(t - t')}$, which is the Green's function for the operator $L_{k\alpha} = i\hbar \frac{\partial}{\partial t} - (\epsilon_k - i\eta)$, and $L_{k\alpha} c_{k\alpha}^{(0)} = S_{k\alpha}$. Plugging Eq. (13) into the first equation of Eqs. (12) and performing the Fourier transformation on the result, we obtain

$$\left(\omega - \epsilon_\alpha - \Sigma_\alpha^{(0)}(\omega) \right) c_\alpha = \mathscr{S}_\alpha + \sum_{\alpha' \neq \alpha} U \mathscr{F}\{c_{\alpha'}^\dagger c_{\alpha'} c_\alpha\}(\omega), \tag{14}$$

where $\mathscr{S}_\alpha = \sum_{k \in L, R} V_{k\alpha} c_{k\alpha}^{(0)}$, $\Sigma_\alpha^{(0)}(\omega) = \sum_{k \in L, R} \frac{|V_{k\alpha}|^2}{\omega - \epsilon_k + i\eta}$ and $\mathscr{F}\{c_{\alpha'}^\dagger c_{\alpha'} c_\alpha\}(\omega)$ represents the Fourier transform of the triple-product operator $c_{\alpha'}^\dagger(t) c_{\alpha'}(t) c_\alpha(t)$. Eq. (14) can be solved approximately by closing it up to a certain order, which generates the Green's function corresponding to that order.

A. Mean Field Approximation

The simplest way to close Eq. (14) is the mean field approximation: $\{c_{\alpha'}^\dagger c_{\alpha'} c_\alpha\}(\omega) \approx \langle n_{\alpha'} \rangle c_\alpha(\omega)$. Therefore the Green's function under the mean field approximation can be written as

$$G_\alpha^{MF}(\omega) = \frac{1}{\omega - \epsilon_\alpha - \Sigma_\alpha^{(0)} - U \sum_{\alpha' \neq \alpha} \langle n_{\alpha'} \rangle}. \tag{15}$$

The LDOS can be expressed in terms of the mean field Green's function G_α^{MF} as

$$\rho(\omega) = -\frac{1}{\pi} \text{Tr} \, \text{Im} \left(G_\alpha(\omega) \right), \tag{16}$$

where the trace accounts for the summation over all four internal degrees of freedom. The occupation number of the state α is given by

$$\langle n_\alpha \rangle = \frac{1}{2} \int d\omega \, \rho_\alpha(\omega) \left[f_L(\omega) + f_R(\omega) \right] \tag{17}$$

for symmetric barriers.

There is an obstruction to evaluate the Green's function $G_\alpha^{MF}(\omega)$. The expression of $G_\alpha^{MF}(\omega)$ depends on the occupation configuration $\{\langle n_\alpha \rangle\}$ (see Eq. (15)), which in turn itself has to be calculated through the Green's function. This requires solving the Green's function and the occupations simultaneously (see Eq. (15) and Eq. (17)). A self-consistent iterative algorithm is developed as shown below.

- Starting with an initial value of $\langle n_\alpha^0 \rangle$ and calculating the Green's function $G_\alpha^{MF}(\omega)$ from Eq. (15).

- Calculating the value of $\langle n_\alpha \rangle$ from Eq. (17) with $\rho(\omega)$ given by Eq. (16).

- Comparing the new occupation $\langle n_\alpha \rangle$ calculated from step 2 with the initial guess $\langle n_\alpha^0 \rangle$. If the new one $\langle n_\alpha \rangle$ is not sufficiently close to the original guess, we revise our guess by

$$\langle n_\alpha^{new} \rangle = \langle n_\alpha^{old} \rangle + \varepsilon \left(\langle n_\alpha \rangle - \langle n_\alpha^{old} \rangle \right),$$

  where ε is a positive number less than 1.

- Repeating the iterative processes $1 - 3$ until the Green's function $G_\alpha^{MF}(\omega)$ yields the occupation configuration $\{\langle n_\alpha \rangle\}$ which is sufficiently close to the previous input value within a predetermined tolerance level.

The remaining question is how we could be able to give a reasonable initial guess of $\langle n_\alpha^0 \rangle$? Under the deep-level assumption that the resonant level ϵ_α is deep well below the chemical potential μ, the LDOS $\rho_\alpha(\omega)$ in Eq. (16) is integrated up to its extreme right side of the tail. Therefore we can choose $\langle n_\alpha^0 \rangle = 1$ as a proper initial guess of the occupations in the self-consistent calculation.

For each internal state with finite U, we find that all single-particle resonances are shifted away from ϵ_α to $\epsilon_\alpha + U \sum_{\alpha' \neq \alpha} \langle n_{\alpha'} \rangle$, as shown in Fig. 2. The imaginary part of self-energy $\Sigma_\alpha^{(0)}$ gives rise to the total energy level broadening in the LDOS.
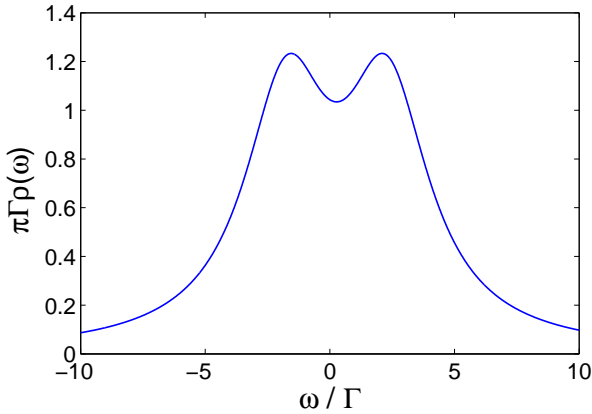

FIG. 2: Density of states $\rho(\omega)$ for TIQDs symmetrically coupled to two external leads with parameters $U = 0.1\Gamma$ and $\epsilon_\alpha = \pm 2\Gamma$. Two leads' chemical potential is set to be $\mu_L = \mu_R = 8\Gamma$. Under the mean field approximation, two distinct peaks are shifted away from the original resonances $\pm 2\Gamma$ to the new ones $\pm 2\Gamma \mp U\langle n \rangle$ in the LDOS.

The mean field approximation is valid only when $k_B T$ or Γ_α is comparable to U, where $\Gamma_\alpha = \pi |V_{k\alpha}|^2 \rho_0$ is the hybridization strength between a TIQD and two external leads. The mean field approximation provides an acceptable description when U is small or temperature

is high. However in real experimental setups, the on-site Coulomb interaction U is typically about the order of several meV, while both the hybridization strength Γ and the temperature $k_B T$ are typically of the order of several μeV. Therefore the mean field approximation discussed in this section does not even provide a qualitatively reliable scheme within the regimes for most of the experimental setups. This requires us to obtain a theory beyond the mean field approximation, which we are going to discuss in the following.

B. Coulomb Blockade Regime

When the Coulomb interaction strength U between localized electrons exceeds both the temperature $k_B T$ and the hybridization strength Γ, the Coulomb blockade effect is dominant in this regime provided that $T < T_K$. One has to truncate the equations of motion up to next-to-leading order in order to close Eq. (14). The corresponding Green's function is derived in Appendix A:

$$G_\alpha^{CB}(\omega) = \frac{1 - \sum_{\alpha' \neq \alpha} \left(\frac{\langle n_{\alpha'} \rangle}{\mathscr{N}_{\alpha'}^{(\alpha)}} \right)}{\omega - \epsilon_\alpha - \Sigma_\alpha^{(0)}} + \sum_{\alpha' \neq \alpha} \frac{\left(\frac{\langle n_{\alpha'} \rangle}{\mathscr{N}_{\alpha'}^{(\alpha)}} \right)}{\omega - \epsilon_\alpha - U\mathscr{N}_{\alpha'}^{(\alpha)} - \Sigma_\alpha^{(0)}},$$

(18)

where $\mathscr{N}_{\alpha'}^{(\alpha)} \equiv 1 + \sum_{\beta \neq \alpha, \alpha'} \langle n_\beta \rangle$, and $\Sigma_\alpha^{(0)}(\omega) = \sum_{k \in L, R} \frac{|V_{k\alpha}|^2}{\omega - \epsilon_k + i\eta}$ is the self-energy term due to tunneling of the α electrons into the leads. The Green's function $G_\alpha^{CB}(\omega)$ in the Coulomb blockade regime has four resonances for each internal channel α. One of them is located at the resonant level ϵ_α weighted by the probability factor $1 - \sum_{\alpha' \neq \alpha} \left(\langle n_{\alpha'} \rangle / \mathscr{N}_{\alpha'}^{(\alpha)} \right)$, and the other three are shifted and located at $\epsilon_\alpha + U\mathscr{N}_\alpha^{(\alpha')}$ weighted by the probability factor $\langle n_{\alpha'} \rangle / \mathscr{N}_\alpha^{(\alpha')}$.

The Green's function $G_\alpha^{CB}(\omega)$ depends on both temperature and chemical potential through the occupation configuration $\{\langle n_\alpha \rangle\}$ in general. The occupations have to be computed via the self-consistent algorithm with constraints $\langle n_1 \rangle = \langle n_2 \rangle$ and $\langle n_3 \rangle = \langle n_4 \rangle$ as discussed in the previous section. To determine a reasonable guess of an initial $\langle n_\alpha^0 \rangle$, we assume that the resonant level ϵ_α of TIQDs is deep enough below the chemical potential μ: $|\mu - \epsilon_\alpha| >> |\epsilon_\alpha|$. We further assume that the occupations of four internal states are all identical, i.e. $\langle n_\alpha \rangle \equiv \langle n \rangle$, $\forall \alpha = 1, 2, 3, 4$ in order to accelerate the iterative processes in the self-consistent computation. It is the Coulomb interaction energy U that dominates all the energy scales in this regime. Therefore only one single resonant level ϵ_α is occupied, while the energy levels of unoccupied states are raised by $U\mathscr{N}$. Double occupancy is energetically costly and hence is forbidden in the large U limit. All unoccupied levels are pushed outside the chemical potential in this limit, and the occupied levels are the only ones contributing to the occupations. This

leads to an equation for the initial guess of the occupation number $\langle n^0 \rangle$:

$$\langle n^0 \rangle = 1 - \sum_{\alpha' \neq \alpha} \frac{\langle n^0 \rangle}{1 + \sum_{\beta \neq \alpha, \alpha'} \langle n^0 \rangle}. \qquad (19)$$

The solution of Eq. (19) reads $\langle n^0 \rangle = \frac{1}{2}\left(\sqrt{3}-1\right)$. This solution turns out to work quite well as a clever initial guess of the occupation configuration $\{\langle n_\alpha \rangle\}$ for the self-consistent algorithm. The occupations will eventually converge to certain consistent values after several iterative steps. After obtaining the self-consistent occupation numbers, the corresponding Green's function in the Coulomb blockade regime can be inferred through Eq. (18). Under the assumption that all the occupations are the same, three shifted resonances $\epsilon_\alpha + U \mathcal{N}_\alpha^{(\alpha')}$ ($\alpha' \neq \alpha$) in $G_\alpha^K(\omega)$ are degenerate to be one located at $\epsilon_\alpha + U(1 + 2\langle n \rangle)$ for each index α. Therefore one shall expect that the corresponding LDOS exhibits four split Coulomb peaks at $\omega = \pm|\epsilon|$ and $\omega = \pm|\epsilon| + U(1 + 2\langle n \rangle)$ respectively, when the hybridization strength Γ is not too strong compared to the QD's absolute energy level $|\epsilon_\alpha|$ as indicated in Fig 3(a).

In principle a four-peak structure should occur in the LDOS when all the occupation numbers are nearly the same. However only two peaks, split by the amount of $U\mathcal{N}$, remain when the hybridization strength Γ exceeds a critical value $\Gamma_c \approx |\epsilon_\alpha|$ as shown in Fig. 3(b). The suppression of peak numbers follows from the fact that the hybridization strength Γ characterizes the level broadening of each discrete eigenstate caused by the coupling between the TIQD and two external leads. When the hybridization strength Γ is made to be greater than Γ_c, the LDOS spreads out around the original resonant peaks due to the level broadening. As a result, two peaks at $\omega = \pm\epsilon$ are merged together as well as the other two peaks located at $\omega = \pm\epsilon + U\mathcal{N}$. We conclude that there exists a continuous crossover from a four-peak structure to a double-peak structure in the LDOS as the hybridization strength Γ increases in the Coulomb blockade regime.

In summary, when Γ is relatively small compared to $|\epsilon_\alpha|$, we find Coulomb peaks form pairs with large inter-pair spacing ($\sim U\mathcal{N}$) and small intra-pair spacing ($\sim |\epsilon_\alpha|$) within the Coulomb blockade regime. Two intra-pair peaks have comparable width and height, while the height of inter-pair peaks is usually different. As the hybridization strength Γ is increased above the critical value Γ_c, the intra-pair peaks merge together, nevertheless two inter-pair peaks still remain in the LDOS. Since electric conductance is proportional to the LDOS at low temperatures, similar features should be expected to be observed in the electric conductance measurement as well. The separation between the conductance's inter-pair peaks is set by the large on-site Coulomb interaction energy, whereas the separation between the intra-pair peaks is determined by the QD's absolute energy level. In the Coulomb blockade regime, a transition from
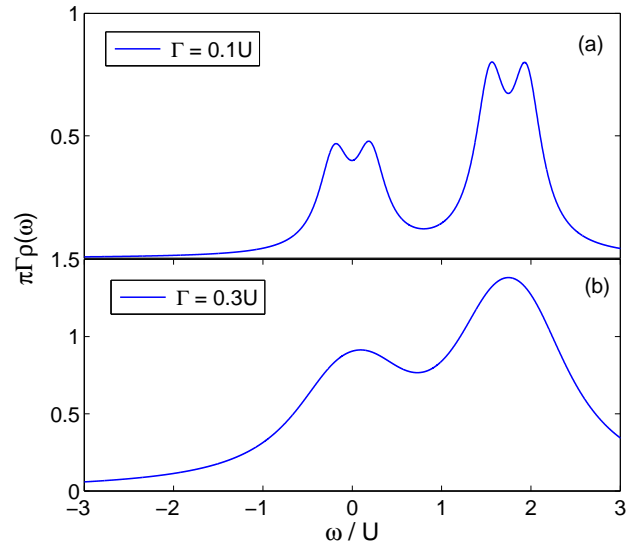

FIG. 3: Local density of states $\pi\Gamma\rho(\omega)$ vs energy ω in units of U in the Coulomb blockade regime with the hybridization strength (a) $\Gamma < \Gamma_c$ and (b) $\Gamma > \Gamma_c$. (a) The LDOS exhibits a quadruple-peak structure at $\epsilon = \pm0.2U$ and $\epsilon = \pm0.2U + (1 + 2\langle n \rangle)U$ in the weak coupling limit ($\Gamma = 0.1U$). The occupations $\langle n \rangle$ converges to 0.3670 via the self-consistent algorithm. (b) Four Coulomb peaks merge into a double-peak structure when the hybridization strength Γ is above the critical value $\Gamma_c \approx 0.2U$ in the strong coupling limit ($\Gamma = 0.3U$).

weak to strong coupling between localized and conduction electrons results a crossover from a quadruple-peak structure to a double-peak structure in the LDOS and electric conductance.

C. Kondo Effect Regime

In this section, our aim is to calculate the transport current through a TIQD as well as the corresponding differential conductance via the self-consistent EOM method in the Kondo regime.

1. Renormalization Group Analysis

In the framework of the renormalization group (RG), high-energy degrees of freedom are successively integrated out and one obtains a low-energy effective theory eventually. A poor-man's scaling approach based on the RG analysis is applied to study the low-energy properties of Hamiltonian (11). The key idea is to integrate out high-energy modes in the interval $[D, D_0]$, where the cutoff D might be the band width of conduction electrons, and rescale all energies and fields appropriately

to construct a new effective Hamiltonian $H(D)$. The RG method relies on the fact that all physical quantities should solely depend on the effective low energy scales such as the Kondo temperature T_K. The band cutoff D should be irrelevant and does not appear in any physically observable quantity. As a consequence, it is possible to absorb the cutoff D into renormalized coupling constants by the requirement that physically observable quantities are invariant under the RG rescaling, leading to the emergence of new energy scales.

First of all, the original Hamiltonian(11) can be rewritten as

$$H = \sum_{\alpha,k\in L,R} \epsilon_k c_{k\alpha}^\dagger c_{k\alpha} + \sum_\alpha \epsilon_\alpha c_\alpha^\dagger c_\alpha \qquad (20)$$
$$+ \sum_{\alpha,k\in L,R} \left(V c_\alpha^\dagger c_{k\alpha} + H.c. \right) + \frac{1}{2}U\left(N - \frac{1}{2} \right)^2 - \frac{1}{8}.$$

where $N \equiv \sum_{\alpha=1}^4 n_\alpha$ is the total number operator, and we assume that all internal degrees of freedom in the TIQD are equally coupled to two external leads, i.e. $V_{k1} = V_{k2} = V_{k3} = V_{k4} \equiv V$.

We now investigate the limit of $U \to \infty$. In this case, only one electron is accommodated in the whole TIQD system. We obtain the following effective Kondo-type Hamiltonian after performing a Schriffer-Wolf transformation:[66]

$$H_K = \sum_{\alpha,k\in L,R} \epsilon_k c_{k\alpha}^\dagger c_{k\alpha} + J[\mathbf{S} \cdot \left(\Psi_r^\dagger \sigma \Psi_r \right)$$
$$+ \left(\Psi_r^\dagger \tau \Psi_r \right) \cdot \mathbf{T} + \mathbf{S} \cdot \left(\Psi_r^\dagger \sigma\tau \Psi_r \right) \cdot \mathbf{T}], \quad (21)$$

where $\Psi_k^\dagger = \left(c_{k1}^\dagger, c_{k2}^\dagger, c_{k3}^\dagger, c_{k4}^\dagger \right)$ is the spinnor of the conduction electrons in two leads and $\Psi_r^\dagger \equiv \sum_k \Psi_k^\dagger$. Similarly, the field operator for the TIQD is defined as $\Psi_d^\dagger \equiv \left(c_1^\dagger, c_2^\dagger, c_3^\dagger, c_4^\dagger \right)$. $\mathbf{S}$ is the spin operator for the TIQD defined as $\mathbf{S} \equiv \Psi_d^\dagger \sigma \Psi_d$, while $\mathbf{T} \equiv \Psi_d^\dagger \tau \Psi_d$ defines the orbital pseudo-spin operator. σ (τ) are Pauli matrices operating on the spin (pseudo-spin) space respectively. The effective coupling constant J in the infinity U limit is initially given by $J = \frac{|V|^2}{|\mu - \epsilon_d|}$ and the corresponding scaling equation up to the second order in J reads

$$\frac{dJ}{d\ln D} = -4\tilde{\rho}_0 J^2, \qquad (22)$$

where $\tilde{\rho}_0$ is the DOS of external leads and D is the renormalization energy cutoff. The coupling constant J exponentially flows into the strong coupling limit as reducing the cutoff D. This reflects a four-fold degeneracy among spin and pseudo-spin degrees of freedom. We notice that Hamiltonian (21) is the renowned $SU(4)$ Kondo Hamiltonian, where the spin and orbital pseudo-spin degrees of freedom are entangled due to the presence of the third term in Eq. (21). Physically, the spin-orbital entanglement is realized naturally in the TI system through its unique spin-orbital locking phenomena. It avoids the possible fine-tuning requirement faced by the DQD and CNQD system. The corresponding Kondo temperature is given by $T_K \approx D \exp\left(-1/4\tilde{\rho}_0 J \right)$. Similar results have been examined in carbon nanotube systems[13], vertical quantum dots systems[26,67], grain-dot systems[27] and parallel double quantum dots systems[31,68,69]. This discussion based on the RG analysis demonstrates the existence of $SU(4)$ Kondo states in the TIQD. In the next section, we show that the LDOS and differential conductance would indicate the main features of spin-orbital Kondo physics, which can be used as experimental probes to detect the spin-orbital Kondo effect in the TIQD system.

2. Local Density of States and Differential Conductance

Before we start to calculate any relevant physical quantities, let us discuss several important characteristic energy scales in the Kondo regime. The depth of a QD's energy level ϵ_α relative to the chemical potential μ is one of these characteristic scales. It is defined as $\Delta\epsilon_{dep} \equiv |\mu - \epsilon_\alpha|$. One requirement of the emergence of Kondo physics is that the hybridization strength Γ has to be smaller than this energy scale $\Delta\epsilon_{dep}$. Otherwise localized electrons can spread from the QD into the leads without applying external voltage. Charge quantization is completely lost even at zero temperature due to this spread-out effect. Therefore the condition $\Gamma < \Delta\epsilon_{dep}$ has to be held in the Kondo regime. Another characteristic energy scale determining the Kondo effect is the Kondo temperature: T_K. The hybridization strength and on-site Coulomb interaction give rise to the Kondo physics only if the temperature is comparable to or lower than the Kondo temperature, i.e. $k_B T < k_B T_K$. On the other hand, the hybridization strength Γ cannot be too small, otherwise the conduction electrons from the leads would be completely trapped in the QD and no transport would occur. This requires Γ to be large enough to overcome the Kondo temperature $k_B T_K$. In summary, the characteristic energy scales have a hierarchical structure: $k_B T < k_B T_K < \Gamma < \Delta\epsilon_{dep}$ in the Kondo physics regime. On-site Coulomb repulsive interaction U is the last significant characteristic energy scale. In most experimental setups, $U \approx 1 meV$ and $\Gamma \approx 1 - 10\mu eV$. It means that the on-site Coulomb interaction U is several orders of magnitude larger than the hybridization strength Γ in reality and hence is the largest energy scale in the Kondo regime. U is typically set to be infinity in theory in order to forbid possible double occupancy. This limit is consistent with the vast majority of experimental setups for the QD systems.

As shown in the RG analysis, the Kondo temperature T_K for the $SU(4)$ Kondo-type model is enhanced exponentially by a factor of 2, comparing to the con-

ventional single-level $SU(2)$ Anderson model. An estimation for the Kondo temperature in the enhanced Kondo regime is $T_K \approx De^{-\pi|\mu-\epsilon_\alpha|/4\Gamma_\alpha}$ (see Eq. (22)), where D is the band width cutoff and Γ_α is the hybridization strength. In addition, we take the conduction band of two symmetric leads to be flat with width $2W$, so the DOS of two external leads is given by $\tilde{\rho}(\omega) = \tilde{\rho}_0 = 1/(2W)$ for $|\omega| < W$. Thus the hybridization strength for each lead could be rewritten as $\Gamma_\alpha^{L/R}(\omega) = 2\pi \sum_{k\in L/R} |V_{k\alpha}|^2 \delta(\omega - \epsilon_{k\alpha}) = 2\pi\tilde{\rho}_0|V_{k\alpha}|^2$. It is convenient to re-define a modified hybridization strength as $\Gamma_\alpha = \Gamma_\alpha^L\Gamma_\alpha^R/\left(\Gamma_\alpha^L + \Gamma_\alpha^R\right) = \pi\tilde{\rho}_0|V_{k\alpha}|^2$, serving as a unit of energy in the following discussion.

The LDOS of TIQDs can be calculated via the non-equilibrium Green's function (see Eq. (16)). We combine the EOM method and the self-consistent algorithm to calculate a consistent Green's function $G^K(\omega)$ in the Kondo regime as shown in Appendix B. Numerical computations based on the non-equilibrium Green's function have been extremely useful to present a quantitative reliable picture of low temperature, non-equilibrium transport through a QD.[4,13,64,65] In this section, we derive a non-equilibrium Green's function based on the self-consistent EOM method to produce the LDOS and non-linear differential conductance in the Kondo regime. The full non-equilibrium Green's function is given by Eq. (B10) as derived in Appendix B. In the infinite-U limit, it can be simplified and reduced to the form:

$$G_\alpha^K(\omega) = \frac{1 - \sum_{\alpha'\neq\alpha} \frac{\langle n_{\alpha'}\rangle}{\mathcal{N}_{\alpha'}^{(\alpha)}}}{\omega - \epsilon_\alpha - \Sigma_\alpha^{(0)} - \sum_{\alpha'\neq\alpha} \frac{1}{\mathcal{N}_{\alpha'}^{(\alpha)}} \tilde{\Sigma}_{\alpha'\alpha}^{(2)}},$$

with

$$\Sigma_\alpha^{(0)}(\omega) = \sum_{k\in L,R} \frac{|V_{k\alpha}|^2}{\omega - \epsilon_k + i\eta},$$

$$\tilde{\Sigma}_{\alpha'\alpha}^{(2)}(\omega) = \sum_{k\in L,R} \frac{|V_{k\alpha'}|^2 f_{k\alpha'}}{\omega - \epsilon_\alpha + \epsilon_{\alpha'} - \epsilon_k + i\eta}, \quad (23)$$

where $f_{k\alpha'}$ is the Fermi-Dirac distribution in the left/right lead. The overall amplitude of the non-equilibrium Green's function $G_\alpha^K(\omega)$ is proportional to the factor $1 - \sum_{\alpha'\neq\alpha} \frac{\langle n_{\alpha'}\rangle}{\mathcal{N}_{\alpha'}^{(\alpha)}}$, where $\langle n_{\alpha'}\rangle$ is the occupation numbers of internal channels other than α, and $\mathcal{N}_{\alpha'}^{(\alpha)} \equiv 1 + \sum_{\beta\neq\alpha,\alpha'} \langle n_\beta \rangle$.

As discussed in the previous section, the occupations have to be computed using the self-consistent algorithm along with the non-equilibrium Green's function Eq. (23). Under the same assumption as in the last section, the initial guess of the occupation numbers can be chosen as $\langle n_\alpha^0 \rangle = \frac{1}{2}(\sqrt{3} - 1)$. After obtaining the final convergent occupation numbers through the iterative process, the corresponding Green's function Eq. (23) can be automatically computed without any ambiguity.

The terms, $\Sigma_\alpha^{(0)}(\omega)$ and $\tilde{\Sigma}_{\alpha'\alpha}^{(2)}(\omega)$, in Eq. (23) are the self-energies due to the coupling to the leads. The loca-

tions of Kondo resonances are totally determined by the poles of Green's function. Since $Re\{\Sigma_\alpha^{(0)}(\omega)\} = 0$, the self-energy $\Sigma_\alpha^{(0)}(\omega)$ has no contribution to the poles. It is the other self-energy term, $\tilde{\Sigma}_{\alpha'\alpha}^{(2)}(\omega)$, that gives rise to the Kondo resonances in the non-equilibrium LDOS. Because the Fermi-Dirac distribution $f_{k\alpha'}$ has an abrupt change near the chemical potential $\mu_{L,R}$ at low temperature, $Re\{\tilde{\Sigma}_{\alpha'\alpha}^{(2)}(\omega)\}$ has single-particle resonances, which are logarithmically divergent at $\omega = \mu_{L,R}$ and $\omega = \mu_{L,R} + 2\epsilon_\alpha$. It produces the Kondo resonances in the LDOS near those energies. The equilibrium LDOS for each internal channel α: $\rho_\alpha(\omega) = -\frac{1}{\pi} Im\left(G_\alpha^K(\omega)\right)$ displays a double-peak structure. One peak is located at chemical potential $\mu = \mu_L = \mu_R$, and another is shifted away from the chemical potential by $2\epsilon_\alpha$. The peak moves downwards for those negative energy states $(\alpha = 1, 2)$ and upwards for those positive energy states $(\alpha = 3, 4)$ as shown in Fig. 4(a),(b). As a bias voltage $\Delta\mu$ is applied, two Kondo peaks are split into pairs, leading to a quadruple-peak structure exhibited in the non-equilibrium LDOS. In this case, two original Kondo peaks in the equilibrium LDOS are further split into pairs spaced by the chemical potential difference $\Delta\mu$. For each state index α, four Kondo peaks appear near $\omega = \mu_{L,R}$ and $\omega = \mu_{L,R} + 2\epsilon_\alpha$ as shown in Fig. 4(c),(d). A new energy scale, the Kondo peak broadening Δb, emerges. The size of Δb is about the same magnitude as the Kondo temperature $k_B T_K$, which can serve as a practical tool to determine the Kondo temperature experimentally.

Our goal is to calculate the electric current I through the TIQD. I can be expressed in terms of the non-equilibrium Green's function and the Fermi-Dirac distribution. An exact expression for I follows from the Keldysh formalism:[70]

$$I = \frac{e}{\hbar} \sum_\alpha \int d\omega \left(f_L(\omega) - f_R(\omega)\right) \Gamma_\alpha(\omega) \left(-\frac{1}{\pi} Im G_\alpha^K(\omega)\right),$$
$$(24)$$

where $\Gamma_\alpha(\omega) = \pi\rho_0|V_{k\alpha}|^2$, and $f_{L/R}(\omega) \equiv f(\omega - \mu_{L/R})$ is the Fermi-Dirac distribution function for left/right lead with $\mu_L = \mu_R + \Delta\mu$. The differential conductance σ_d is sequentially defined as differentiating the current I with respect to the applied bias voltage $\Delta\mu$: $\sigma_d \equiv e\frac{dI}{d\Delta\mu}$. σ_d is an experimentally observable quantity and can be used as a means of detection to Kondo physics.

The non-linear differential conductance σ_d exhibits a triple-peak structure for temperatures below the Kondo temperature $k_B T_K$ as shown in Fig. 5. This can be explained intuitively through so called "matching mechanism". As discussed previously, Kondo resonances are located at $\omega = \mu_{L,R}$ and $\omega = \mu_{L,R} \pm 2|\epsilon_\alpha|$ in the non-equilibrium LDOS. The differential conductance σ_d is enhanced if and only if three Kondo peaks in the left-lead's LDOS matches the other three peaks in the right-lead's LDOS. Accordingly, a triple-peak structure appears in the differential conductance at $\Delta\mu = 0$ and $\Delta\mu = \pm 2|\epsilon_\alpha|$
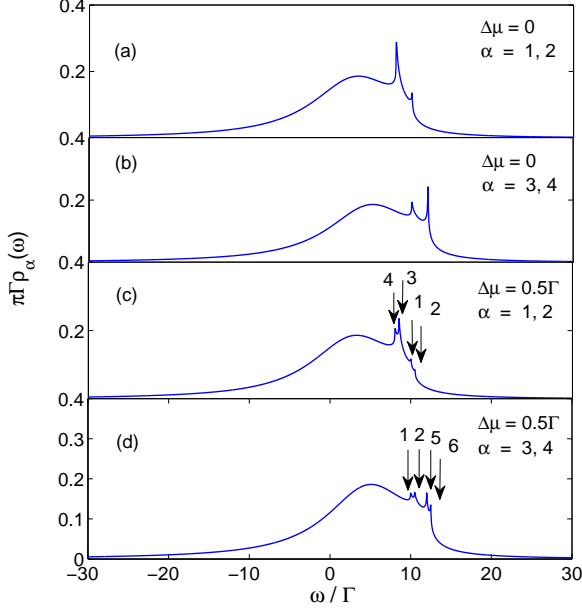
FIG. 4: Local Density of states $\pi\Gamma\rho_\alpha(\omega)$ for a TIQD symmetrically coupled to two external leads with the chemical potential μ_L and μ_R in the limit of $U \to \infty$. The TIQD is prepared to have four internal states with levels $\epsilon_{1,2} = -\Gamma$ and $\epsilon_{3,4} = \Gamma$. Temperature is set to be $T = 0.01\Gamma$, while the Kondo temperature is roughly estimated to be $T_K \approx 0.08\Gamma$. (a) and (b) display the equilibrium ($\mu_L = \mu_R = 10\Gamma$) LDOS for negative levels $\epsilon_{\alpha=1,2}$ (a) and positive levels $\epsilon_{\alpha=3,4}$ (b). It exhibits a double-peak structure at $\omega = 10\Gamma$ and $\omega = 9\Gamma$ for (a) and at $\omega = 10\Gamma$ and $\omega = 11\Gamma$ for (b). (c) and (d) are the non-equilibrium LDOS for negative energy states (c) and positive energy states (d). Four Kondo peaks emerge in the non-equilibrium LDOS. Two of them are located at each lead's chemical potential: $\mu_L = 10.5\Gamma$, $\mu_R = 10\Gamma$ (arrows 1 and 2), and the other two peaks are shift either downwards from the chemical potential by -2Γ ($= -2|\epsilon_\alpha|$) (arrows 3 and 4 in (c)) or upwards from the chemical potential by 2Γ ($= 2|\epsilon_\alpha|$) (arrows 5 and 6 in (d)).

respectively. As the chemical potential is shifted away from the Kondo peaks, the differential conductance σ_d falls off rapidly once the mismatch between two external leads exceeds the Kondo peak broadening Δb. This means that the full width at half maximum (FWHM) of the differential conductance linewidth should have the same order of magnitude as the peak broadening Δb of the LDOS. The triple-peak structure in the differential conductance disappears as the temperature is raised above the Kondo temperature due to the complete destruction of Kondo states when $T > T_K$ as shown in dashed line in Fig. 5. The experimental Observation of this triple-peak structure in the differential conductance was reported recently in parallel DQD systems when the orbital degeneracy is artificially lifted.[38]

Next, we provide a more rigorous theoretical treatment of differential conductance, and demonstrate that the differential conductance σ_d is closely related to the summa-
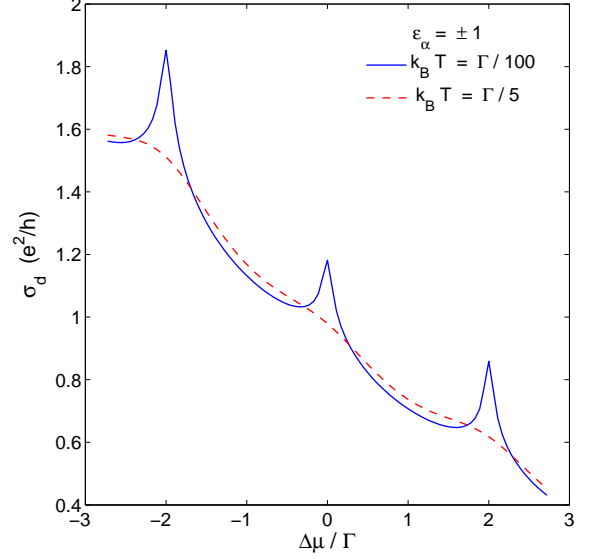

FIG. 5: Differential conductance as a function of the applied bias voltage $\Delta\mu$ in units of e^2/h via the EOM method for the temperatures above T_K (solid line) and below T_K (dashed line). When $\Delta\mu$ is adjusted so that the Kondo peaks in the left lead's DOS coincides with those in the right lead's DOS, the differential conductance σ_d is enhanced. It shows a triple-peak structure at $\Delta\mu = 0$ and $\Delta\mu = \pm2|\epsilon_\alpha| = \pm2\Gamma$ (solid line). When the temperature is raised above the Kondo temperature T_K, the triple-peak structure in the differential conductance disappears as shown in dashed line.

tion of LDOS over all four internal conduction channels. Hence the peak structure in the differential conductance is determined by the corresponding peak structure in the LDOS. In particular, the zero-temperature current I can be calculated as an integral of LDOS over the interval $[\mu_R, \mu_L]$, weighted by the hybridization strength $\Gamma_\alpha(\omega)$. Therefore we can obtain an exact expression for the differential conductance in terms of the single-particle LDOS in the zero-temperature limit:

$$\sigma_d = \frac{e^2}{h} 2\pi\Gamma \int d\omega \left(-\frac{\partial f(\omega - \mu_R - \Delta\mu)}{\partial\omega} \right) \sum_\alpha \rho_\alpha(\omega). \tag{25}$$

We notice that $-\frac{\partial f(\omega)}{\partial\omega}$ becomes a Dirac delta-function when $T \to 0$, so we can rewrite Eq. (25) as

$$\sigma_d^{T=0}(\Delta\mu) \cong \frac{e^2}{h} 2\pi\Gamma \sum_\alpha \rho_\alpha(\mu_R + \Delta\mu). \tag{26}$$

Eq. (26) connects the nonlinear differential conductance at zero temperature to the summation of LDOS over four internal degrees of freedom. In this limit, the peak structure of the differential conductance depends on the value of the corresponding LDOS at $\mu_R + \Delta\mu$, leading to a

condition for the peak structure of the differential conductance:

$$\mu_R + \Delta\mu = \mu_{R,L}, \mu_{R,L} \pm 2|\epsilon_\alpha|. \tag{27}$$

Three cases need to be discussed separately:

Case (1): $\mu_R + \Delta\mu = \mu_L$. This condition is trivially satisfied. It illustrates the existence of the overall background conductance in σ_d, which is independent of the applied bias voltage $\Delta\mu$.

Case (2): $\mu_R + \Delta\mu = \mu_L \pm 2|\epsilon_\alpha|$. There is no solution can be found in this case.

Case (3): $\mu_R + \Delta\mu = \mu_R$ or $\mu_R \pm 2|\epsilon_\alpha|$. This is the most interesting condition, where three solutions exist: $\Delta\mu = 0, \pm 2|\epsilon_\alpha|$. These three solutions correspond exactly to the locations of the three peaks built upon the background conductance in σ_d as depicted in Fig. 5. The result agrees with our intuitive argument as well as the general numerical calculation. Although the analysis is performed in the zero temperature limit, the triple-peak structure still preserves for temperatures below the Kondo temperature T_K.

This discussion demonstrates the existence of spin-orbital Kondo states in TIQD systems. One of the advantages of such devices is that it can potentially avoid the fine-tuning between intradot and iterdot charging energies in DQDs or the fine-tuning between spin and wrapping modes in CNQDs. We also prove that the differential conductance σ_d, as an experimental measurable quantity, indicates the principal features of spin-orbital Kondo effect. The fact that the spin-orbital Kondo states can be observed in TIQD systems as a triple-peak structure in the non-linear differential conductance is important, since it could serve as a means of experimental detection of spin-orbital Kondo physics.

IV. SUMMARY AND CONCLUSIONS

In this paper we investigate the non-equilibrium transport properties of TIQDs in the Coulomb blockade and Kondo regime. An Anderson-type model, which describes the low temperature transport properties through a QD, is derived. We illustrate that the corresponding Anderson impurity Hamiltonian realizes the spin-orbital Kondo effect due to the intrinsic spin-orbital entanglement in TI materials. We conclude that TIQDs can be used to study the spin-orbital Kondo effect in addition to conventional DQD or CNQD systems.

We demonstrate that the mean field approximation is not applicable to the energy scales related to the Coulomb blockade or Kondo regime. A continuous crossover of peak structures controlled by the hybridization strength is found in the Coulomb blockade regime. As the hybridization strength Γ is raised above a critical value Γ_c, the intra-pair peaks are merged together so that only two inter-pair peaks remain in the LDOS. A transition from a quadruple-peak to a double-peak structure occurs when the hybridization strength Γ increases. A similar crossover phenomena is also expected to be observed in the transport measurements in the Coulomb blockade regime. For temperatures below the Kondo temperature T_K, we have shown the emergence of four Kondo peaks in the non-equilibrium LDOS for each conduction channel α. Two of them are located at the chemical potential $\mu_{L/R}$, while the other two peaks are shifted away from the chemical potential by the amount of $2\epsilon_\alpha$. This result leads to the experimental prediction of a triple-peak structure in the differential conductance σ_d provided that the energy hierarchy $k_B T < k_B T_K < \Gamma < \Delta\epsilon_{dep} \ll U$ is satisfied. The triple-peak feature vanishes when the temperature is high enough to break the spin-orbital Kondo states. In contrast to conventional DQD or CNQD systems, no fine-tuning of experimental parameters is necessary in TIQD setups in order to realize the $SU(4)$ Kondo effect. Therefore TIQD systems provide a more controllable platform to investigate the spin-orbital Kondo effect.

An interesting issue not discussed in this paper is the Kondo physics in TIQD systems when a finite magnetic filed is applied. Since the symmetry protected edge states are no longer stable in the presence of an external magnetic field, we expect a totally different transport behavior in comparison with the usual DQD or CNQD systems. Our paper is just the first step to understand the spin-orbital Kondo physics associated with TIQDs. Further investigations regarding the spin-orbital Kondo effect in TIQDs under an external magnetic field are demanded for future research.

Appendix A: Green's Function within Coulomb Blockade Regime

In this section, we present a derivation of the Green's function $G^{CB}(\omega)$ within the Coulomb blockade regime. We start from Eq. (14) and notice that the expression of Eq. (14) is not closed yet because of the presence of a triple-product operator: $c_{\alpha'}^\dagger(t)c_{\alpha'}(t)c_\alpha(t)$. Therefore we differentiate the triple-product operator with respect to time in order to close the equations-of-motion. The final result is given by

$$
\begin{aligned}
i\hbar\frac{\partial}{\partial t}\left(c_{\alpha'}^\dagger c_{\alpha'} c_\alpha\right) = & \ -\left(-i\hbar\frac{\partial c_{\alpha'}^\dagger}{\partial t}\right)c_{\alpha'}c_\alpha + c_{\alpha'}^\dagger\left(i\hbar\frac{\partial c_{\alpha'}}{\partial t}\right)c_\alpha + c_{\alpha'}^\dagger c_{\alpha'}\left(i\hbar\frac{\partial c_\alpha}{\partial t}\right) \\
= & \ \epsilon_\alpha c_{\alpha'}^\dagger c_{\alpha'} c_\alpha + \sum_{k\in L,R}\left(-V_{k\alpha'}^* c_{k\alpha'}^\dagger c_{\alpha'} c_\alpha + V_{k\alpha'}c_{\alpha'}^\dagger c_{k\alpha'} c_\alpha + V_{k\alpha}c_{\alpha'}^\dagger c_{\alpha'} c_{k\alpha}\right) + U\sum_{\beta\neq\alpha}c_{\alpha'}^\dagger c_{\alpha'}c_\alpha c_\beta^\dagger c_\beta \\
\approx & \ \left(\epsilon_\alpha + U + U\left(\sum_{\beta\neq\alpha,\alpha'}\langle n_\beta\rangle\right)\right)c_{\alpha'}^\dagger c_{\alpha'}c_\alpha + \sum_{k\in L,R}\left(V_{k\alpha}c_{\alpha'}^\dagger c_{\alpha'}c_{k\alpha}\right),
\end{aligned}
\tag{A1}
$$

where we ignore the contributions coming from terms $c_{k\alpha'}^\dagger c_{\alpha'} c_\alpha$ and $c_{\alpha'}^\dagger c_{k\alpha'} c_\alpha$ (notice $\alpha\neq\alpha'$) up to the first-order approximation. The Fourier transform of Eq. (A1) reads

$$
\left(\omega - \epsilon_\alpha - U\left(1+\sum_{\beta\neq\alpha,\alpha'}\langle n_\beta\rangle\right)\right)\mathscr{F}\{c_{\alpha'}^\dagger c_{\alpha'}c_\alpha\}(\omega) = \sum_{k\in L,R}V_{k\alpha}\mathscr{F}\{c_{\alpha'}^\dagger c_{\alpha'}c_{k\alpha}\}(\omega),
\tag{A2}
$$

where $\mathscr{F}\{...\}$ represents the Fourier transform of any operator inside the curly bracket.

Eq. (A2) still does not close the equations-of-motion because of the presence of another triple-product term $c_{\alpha'}^\dagger c_{\alpha'} c_{k\alpha}$. Hence one has to further take the time derivative over this triple-product:

$$
\begin{aligned}
i\hbar\frac{\partial}{\partial t}\left(c_{\alpha'}^\dagger c_{\alpha'} c_{k\alpha}\right) = & \ -\left(-i\hbar\frac{\partial c_{\alpha'}^\dagger}{\partial t}\right)c_{\alpha'}c_{k\alpha} + c_{\alpha'}^\dagger\left(i\hbar\frac{\partial c_{\alpha'}}{\partial t}\right)c_{k\alpha} + c_{\alpha'}^\dagger c_{\alpha'}\left(i\hbar\frac{\partial c_{k\alpha}}{\partial t}\right) \\
= & \ (\epsilon_k - i\eta)c_{\alpha'}^\dagger c_{\alpha'}c_{k\alpha} + \sum_{k'\in L,R}\left(-V_{k'\alpha'}^* c_{k'\alpha'}^\dagger c_{\alpha'} c_{k\alpha} + V_{k'\alpha'}c_{\alpha'}^\dagger c_{k'\alpha'} c_{k\alpha}\right) + V_{k\alpha}^* c_{\alpha'}^\dagger c_{\alpha'}c_\alpha + S_{k\alpha}c_{\alpha'}^\dagger c_{\alpha'} \\
\approx & \ (\epsilon_k - i\eta)c_{\alpha'}^\dagger c_{\alpha'}c_{k\alpha} + V_{k\alpha}^* c_{\alpha'}^\dagger c_{\alpha'}c_\alpha + \langle n_{\alpha'}\rangle S_{k\alpha}.
\end{aligned}
\tag{A3}
$$

The fourier transform of Eq. (A3) gives

$$
\mathscr{F}\{c_{\alpha'}^\dagger c_{\alpha'} c_{k\alpha}\}(\omega) = \frac{V_{k\alpha}^*}{\omega - \epsilon_k + i\eta}\mathscr{F}\{c_{\alpha'}^\dagger c_{\alpha'}c_\alpha\}(\omega) + \langle n_{\alpha'}\rangle c_{k\alpha}^{(0)}(\omega).
\tag{A4}
$$

Substituting Eq. (A4) into Eq. (A2), a closed form is finally obtained as

$$
\mathscr{F}\{c_{\alpha'}^\dagger c_{\alpha'} c_\alpha\}(\omega) = \frac{\langle n_{\alpha'}\rangle}{\omega - \epsilon_\alpha - U\left(1+\sum_{\beta\neq\alpha,\alpha'}\langle n_\beta\rangle\right) - \Sigma_\alpha^{(0)}}\mathscr{S}_\alpha.
\tag{A5}
$$

Plugging Eq. (A5) into the original Eq. (14), one obtains the Green's function in the Coulomb blockade regime as

$$
\begin{aligned}
G_\alpha(\omega)^{CB} = & \ \left(\omega - \epsilon_\alpha - \Sigma_\alpha^{(0)}\right)^{-1}\left(1 + \sum_{\alpha'\neq\alpha}\frac{U\langle n_{\alpha'}\rangle}{\omega - \epsilon_\alpha - U\left(1+\sum_{\beta\neq\alpha,\alpha'}\langle n_\beta\rangle\right) - \Sigma_\alpha^{(0)}}\right) \\
= & \ \frac{1 - \sum_{\alpha'\neq\alpha}\left(\frac{\langle n_{\alpha'}\rangle}{\mathscr{N}_{\alpha'}^{(\alpha)}}\right)}{\omega - \epsilon_\alpha - \Sigma_\alpha^{(0)}} + \sum_{\alpha'\neq\alpha}\frac{\left(\frac{\langle n_{\alpha'}\rangle}{\mathscr{N}_{\alpha'}^{(\alpha)}}\right)}{\omega - \epsilon_\alpha - U\mathscr{N}_{\alpha'}^{(\alpha)} - \Sigma_\alpha^{(0)}},
\end{aligned}
\tag{A6}
$$

where $\mathscr{N}_{\alpha'}^{(\alpha)}\equiv 1+\sum_{\beta\neq\alpha,\alpha'}\langle n_\beta\rangle$.

Appendix B: Green's function within Kondo regime

We derive the Green's function in the Kondo regime in this section. We start from Eq. (14) and apply the equations-of-motion method up to the second-order approximation. The equations-of-motion method is based on the Heisenberg equation, and in this case it consists of differentiating the triple-product operator $c_{\alpha'}^\dagger c_{\alpha'} c_\alpha$ with respect to time. A series of operator-product terms is generated and has to be approximated to certain order in order to close the equations-of-motion eventually. Higher-order approximation is required in order for the emergence of Kondo physics. First of all, we take the time derivative over the triple-product operator $c_{\alpha'}^\dagger c_{\alpha'} c_\alpha$:

$$
\begin{aligned}
i\hbar \frac{\partial}{\partial t}\left(c_{\alpha'}^\dagger c_{\alpha'} c_\alpha\right) = & -\left(-i\hbar\frac{\partial c_{\alpha'}^\dagger}{\partial t}\right) c_{\alpha'} c_\alpha + c_{\alpha'}^\dagger \left(i\hbar\frac{\partial c_{\alpha'}}{\partial t}\right) c_\alpha + c_{\alpha'}^\dagger c_{\alpha'} \left(i\hbar\frac{\partial c_\alpha}{\partial t}\right) \\
= & \ \epsilon_\alpha c_{\alpha'}^\dagger c_{\alpha'} c_\alpha + \sum_{k\in L,R}\left(-V_{k\alpha'}^* c_{k\alpha'}^\dagger c_{\alpha'} c_\alpha + V_{k\alpha'} c_{\alpha'}^\dagger c_{k\alpha'} c_\alpha + V_{k\alpha} c_{\alpha'}^\dagger c_{\alpha'} c_{k\alpha}\right) + U \sum_{\beta\neq\alpha} c_{\alpha'}^\dagger c_{\alpha'} c_\alpha c_\beta^\dagger c_\beta \\
\approx & \ \left(\epsilon_\alpha + U + U\left(\sum_{\beta\neq\alpha,\alpha'}\langle n_\beta\rangle\right)\right) c_{\alpha'}^\dagger c_{\alpha'} c_\alpha + \sum_{k\in L,R}\left(-V_{k\alpha'}^* c_{k\alpha'}^\dagger c_{\alpha'} c_\alpha + V_{k\alpha'} c_{\alpha'}^\dagger c_{k\alpha'} c_\alpha + V_{k\alpha} c_{\alpha'}^\dagger c_{\alpha'} c_{k\alpha}\right),
\end{aligned}
\tag{B1}
$$

where the contributions from terms $c_{k\alpha'}^\dagger c_{\alpha'} c_\alpha$ and $c_{\alpha'}^\dagger c_{k\alpha'} c_\alpha$ are kept in this case. The Fourier transform of Eq. (B1) can be written as

$$
\left(\omega - \epsilon_\alpha - U\left(1 + \sum_{\beta\neq\alpha,\alpha'}\langle n_\beta\rangle\right)\right)\mathscr{F}\{c_{\alpha'}^\dagger c_{\alpha'} c_\alpha\} = \sum_{k\in L,R}\left(-V_{k\alpha'}^*\mathscr{F}\{c_{k\alpha'}^\dagger c_{\alpha'} c_\alpha\} + V_{k\alpha'}\mathscr{F}\{c_{\alpha'}^\dagger c_{k\alpha'} c_\alpha\} + V_{k\alpha}\mathscr{F}\{c_{\alpha'}^\dagger c_{\alpha'} c_{k\alpha}\}\right).
\tag{B2}
$$

In order to close the equations-of-motion, we have to further take the time derivatives over the remaining operator-product terms $c_{k\alpha'}^\dagger c_{\alpha'} c_\alpha$, $c_{\alpha'}^\dagger c_{k\alpha'} c_\alpha$ and $c_{\alpha'}^\dagger c_{\alpha'} c_{k\alpha}$ respectively. We have already obtained the Fourier transform $\mathscr{F}\{c_{\alpha'}^\dagger c_{\alpha'} c_{k\alpha}\}$ from Appendix A as shown in Eq. (A4):

$$
\mathscr{F}\{c_{\alpha'}^\dagger c_{\alpha'} c_{k\alpha}\}(\omega) = \frac{V_{k\alpha}^*}{\omega - \epsilon_k + i\eta}\mathscr{F}\{c_{\alpha'}^\dagger c_{\alpha'} c_\alpha\}(\omega) + \langle n_{\alpha'}\rangle c_{k\alpha}^{(0)}(\omega).
\tag{B3}
$$

The time derivatives over the other two operator-product terms appearing in Eq. (B2) are given by

$$
\begin{aligned}
i\hbar \frac{\partial}{\partial t}\left(c_{k\alpha'}^\dagger c_{\alpha'} c_\alpha\right) = & -\left(-i\hbar\frac{\partial c_{k\alpha'}^\dagger}{\partial t}\right) c_{\alpha'} c_\alpha + c_{k\alpha'}^\dagger \left(i\hbar\frac{\partial c_{\alpha'}}{\partial t}\right) c_\alpha + c_{k\alpha'}^\dagger c_{\alpha'} \left(i\hbar\frac{\partial c_\alpha}{\partial t}\right) \\
= & \ (\epsilon_\alpha + \epsilon_{\alpha'} - \epsilon_k - i\eta)\, c_{k\alpha'}^\dagger c_{\alpha'} c_\alpha - V_{k\alpha'} c_{\alpha'}^\dagger c_{\alpha'} c_\alpha + \sum_{k'\in L,R}\left(V_{k'\alpha'} c_{k\alpha'}^\dagger c_{k'\alpha'} c_\alpha + V_{k'\alpha} c_{k\alpha'}^\dagger c_{\alpha'} c_{k'\alpha}\right) \\
& + \sum_{\beta\neq\alpha'} U c_{k\alpha'}^\dagger c_\beta^\dagger c_\beta c_{\alpha'} c_\alpha + \sum_{\beta\neq\alpha} U c_{k\alpha'}^\dagger c_{\alpha'} c_\beta^\dagger c_\beta c_\alpha - S_{k\alpha'}^* c_{\alpha'} c_\alpha \\
\approx & \ \left(\epsilon_\alpha + \epsilon_{\alpha'} - \epsilon_k + U + 2U\sum_{\beta\neq\alpha,\alpha'}\langle n_\beta\rangle - i\eta\right) c_{k\alpha'}^\dagger c_{\alpha'} c_\alpha - V_{k\alpha'} c_{\alpha'}^\dagger c_{\alpha'} c_\alpha + V_{k\alpha'} f_{k\alpha'} c_\alpha,
\end{aligned}
\tag{B4}
$$

where $f_{k\alpha'}$ is the unperturbed Fermi-Dirac distribution for the leads, and

$$
\begin{aligned}
i\hbar \frac{\partial}{\partial t}\left(c_{\alpha'}^\dagger c_{k\alpha'} c_\alpha\right) = & -\left(-i\hbar\frac{\partial c_{\alpha'}^\dagger}{\partial t}\right) c_{k\alpha'} c_\alpha + c_{\alpha'}^\dagger \left(i\hbar\frac{\partial c_{k\alpha'}}{\partial t}\right) c_\alpha + c_{\alpha'}^\dagger c_{k\alpha'} \left(i\hbar\frac{\partial c_\alpha}{\partial t}\right) \\
= & \ (\epsilon_\alpha - \epsilon_{\alpha'} + \epsilon_k - i\eta)\, c_{\alpha'}^\dagger c_{k\alpha'} c_\alpha + \sum_{k\in L,R}\left(V_{k'\alpha} c_{\alpha'}^\dagger c_{k\alpha'} c_{k'\alpha} - V_{k'\alpha'}^* c_{k'\alpha'}^\dagger c_{k\alpha'} c_\alpha\right) + V_{k\alpha'}^* c_{\alpha'}^\dagger c_{\alpha'} c_\alpha \\
& - \sum_{\beta\neq\alpha'} U c_{\alpha'}^\dagger c_\beta^\dagger c_\beta c_{k\alpha'} c_\alpha + \sum_{\beta\neq\alpha} U c_{\alpha'}^\dagger c_{k\alpha'} c_\beta^\dagger c_\beta c_\alpha + S_{k\alpha'} c_{\alpha'}^\dagger c_\alpha \\
\approx & \ (\epsilon_\alpha - \epsilon_{\alpha'} + \epsilon_k - i\eta)\, c_{\alpha'}^\dagger c_{k\alpha'} c_\alpha - V_{k\alpha'}^* f_{k\alpha'} c_\alpha + V_{k\alpha'}^* c_{\alpha'}^\dagger c_{\alpha'} c_\alpha.
\end{aligned}
\tag{B5}
$$

Then the Fourier transforms of Eqs. (B4) and (B5) can be written as

$$\mathscr{F}\{c^\dagger_{k\alpha'}c_{\alpha'}c_\alpha\}(\omega) = -\frac{V_{k\alpha'}}{\omega - \epsilon_\alpha - \epsilon_{\alpha'} + \epsilon_k - U\left(1 + 2\sum_{\beta\neq\alpha,\alpha'}\langle n_\beta\rangle\right) + i\eta}\mathscr{F}\{c^\dagger_{\alpha'}c_{\alpha'}c_\alpha\}(\omega)$$
$$+\frac{V_{k\alpha'}f_{k\alpha'}}{\omega - \epsilon_\alpha - \epsilon_{\alpha'} + \epsilon_k - U\left(1 + 2\sum_{\beta\neq\alpha,\alpha'}\langle n_\beta\rangle\right) + i\eta}c_\alpha(\omega), \quad (B6)$$

and

$$\mathscr{F}\{c^\dagger_{\alpha'}c_{k\alpha'}c_\alpha\}(\omega) = \frac{V^*_{k\alpha'}}{\omega - \epsilon_\alpha + \epsilon_{\alpha'} - \epsilon_k + i\eta}\mathscr{F}\{c^\dagger_{\alpha'}c_{\alpha'}c_\alpha\}(\omega) - \frac{V^*_{k\alpha'}f_{k\alpha'}}{\omega - \epsilon_\alpha + \epsilon_{\alpha'} - \epsilon_k + i\eta}c_\alpha(\omega). \quad (B7)$$

Substituting Eqs. (B3), (B6) and (B7) into Eq. (B2), we obtain a closed form:

$$\mathscr{F}\{c^\dagger_{\alpha'}c_{\alpha'}c_\alpha\}(\omega) = -\frac{\Sigma^{(2)}_{\alpha'\alpha}}{\omega - \epsilon_\alpha - \Sigma^{(0)}_\alpha - U\mathscr{N}^{(\alpha)}_{\alpha'} - \Sigma^{(1)}_{\alpha'\alpha}}c_\alpha(\omega) + \frac{\langle n_{\alpha'}\rangle}{\omega - \epsilon_\alpha - \Sigma^{(0)}_\alpha - U\mathscr{N}^{(\alpha)}_{\alpha'} - \Sigma^{(1)}_{\alpha'\alpha}}\mathscr{S}_\alpha, \quad (B8)$$

where the self-energy terms are defined as

$$\Sigma^{(0)}_\alpha(\omega) = \sum_{k\in L,R}\frac{|V_{k\alpha}|^2}{\omega - \epsilon_k + i\eta},$$

$$\Sigma^{(1)}_{\alpha'\alpha}(\omega) = \sum_{k\in L,R}\left(\frac{|V_{k\alpha'}|^2}{\omega - \epsilon_\alpha + \epsilon_{\alpha'} - \epsilon_k + i\eta} + \frac{|V_{k\alpha'}|^2}{\omega - \epsilon_\alpha - \epsilon_{\alpha'} + \epsilon_k - U\left(1 + 2\sum_{\beta\neq\alpha,\alpha'}\langle n_\beta\rangle\right) + i\eta}\right),$$

$$\Sigma^{(2)}_{\alpha'\alpha}(\omega) = \sum_{k\in L,R}\left(\frac{|V_{k\alpha'}|^2 f_{k\alpha'}}{\omega - \epsilon_\alpha + \epsilon_{\alpha'} - \epsilon_k + i\eta} + \frac{|V_{k\alpha'}|^2 f_{k\alpha'}}{\omega - \epsilon_\alpha - \epsilon_{\alpha'} + \epsilon_k - U\left(1 + 2\sum_{\beta\neq\alpha,\alpha'}\langle n_\beta\rangle\right) + i\eta}\right). \quad (B9)$$

Finally we substitute Eq. (B8) back into Eq. (14), so we obtain the full Green's function within the Kondo regime:

$$G^K_\alpha(\omega) = \left(\omega - \epsilon_\alpha - \Sigma^{(0)}_\alpha + U\sum_{\alpha'\neq\alpha}\frac{\Sigma^{(2)}_{\alpha'\alpha}}{\omega - \epsilon_\alpha - \Sigma^{(0)}_\alpha - U\mathscr{N}^{(\alpha)}_{\alpha'} - \Sigma^{(1)}_{\alpha'\alpha}}\right)^{-1}\left(1 + U\sum_{\alpha'\neq\alpha}\frac{\langle n_{\alpha'}\rangle}{\omega - \epsilon_\alpha - \Sigma^{(0)}_\alpha - U\mathscr{N}^{(\alpha)}_{\alpha'} - \Sigma^{(1)}_{\alpha'\alpha}}\right)$$

$$= \frac{1 - \sum_{\alpha'\neq\alpha}\frac{\langle n_{\alpha'}\rangle}{\mathscr{N}^{(\alpha)}_{\alpha'}}}{\omega - \epsilon_\alpha - \Sigma^{(0)}_\alpha + U\sum_{\alpha'\neq\alpha}\Sigma^{(2)}_{\alpha'\alpha}\left(\omega - \epsilon_\alpha - \Sigma^{(0)}_\alpha - U\mathscr{N}^{(\alpha)}_{\alpha'} - \Sigma^{(1)}_{\alpha'\alpha}\right)^{-1}}$$

$$+ \sum_{\alpha'\neq\alpha}\frac{\frac{\langle n_{\alpha'}\rangle}{\mathscr{N}^{(\alpha)}_{\alpha'}}}{\omega - \epsilon_\alpha - \Sigma^{(0)}_\alpha - U\mathscr{N}^{(\alpha)}_{\alpha'} - U\left(\mathscr{N}^{(\alpha)}_{\alpha'}\Sigma^{(1)}_{\alpha'\alpha} - \Sigma^{(3)}_{\alpha'\alpha}\right)\left(\omega - \epsilon_\alpha - \Sigma^{(0)}_\alpha - \Sigma^{(1)}_{\alpha'\alpha}\right)^{-1}}, \quad (B10)$$

where the self-energy $\Sigma^{(3)}_{\alpha'\alpha}(\omega)$ is defined as

$$\Sigma^{(3)}_{\alpha'\alpha}(\omega) = \sum_{\beta\neq\alpha}\Sigma^{(2)}_{\beta\alpha}(\omega)\left(\frac{\omega - \epsilon_\alpha - \Sigma^{(0)}_\alpha - U\mathscr{N}^{(\alpha)}_{\alpha'} - \Sigma^{(1)}_{\alpha'\alpha}}{\omega - \epsilon_\alpha - \Sigma^{(0)}_\alpha - U\mathscr{N}^{(\alpha)}_\beta - \Sigma^{(1)}_{\beta\alpha}}\right). \quad (B11)$$

[1] T. K. Ng and P. A. Lee, Phys. Rev. Lett. **61**, 1768 (1988).
[2] P. W. Anderson, Phys. Rev. **124**, 41 (1961).
[3] S. Hershfield, J. H. Davies and J. W. Wilkins, Phys. Rev. Lett. **67**, 3720 (1991).
[4] Y. Meir, N. S. Wingreen and P. A. Lee, Phys. Rev. Lett. **70**, 2601 (1993).

[5] D. Goldhaber-Gordon, H. Shtrikman, D. Mahalu, D. Abusch-Magder, U. Meirav, and M. A. Kastner, Nature **391**, 156 (1998).

[6] S. M. Cronenwett, T. H. Oosterkamp, L. P. Kouwenhoven, Science, **281**, 540 (1998).

[7] S. Sasaki, S. De Franceschi, J. M. Elzerman, W. G. van der Wiel, M. Eto, S. Tarucha, and L. P. Kouwenhoven, Nature **405**, 764 (2000).

[8] W. G. van der Wiel, S. De Franceschi, T. Fujisawa, J. M. Elzerman, S. Tarucha, and L. P. Kouwenhoven, Science **289**, 2105 (2000).

[9] L. J. Klein, D. E. Savage, and M. A. Eriksson, Appl. Phys. Lett. **90**, 033103 (2007).

[10] J. Nygård, D. H. Cobden, and P. E. Lindelof, Nature **408**, 342 (2000).

[11] B. Babic, T. Kontos, and C. Schonenberger, Phys. Rev. B **70**, 235419 (2004).

[12] P. Jarillo-Herrero, J. Kong, Herre S.J. van der Zant, C. Dekker, L. P. Kouwenhoven, and S. De Franceschi, Nature **434**, 484 (2005).

[13] M. -S. Choi, R. Lopez, and R. Aguado, Phys. Rev. Lett. **95**, 067204 (2005).

[14] J. S. Lim, M. S. Choi, M. Y. Choi, R. Lopez, R. Aguado, Phys. Rev. B **74**, 205119 (2006).

[15] T. S. Jespersen, M. Aagesen, C. Sorensen, P. E. Lindelof, and J. Nygard, Phys. Rev. B **74**, 233304 (2006).

[16] C. A. Busser, and G. B. Martins, Phys. Rev. B **75**, 045406 (2007).

[17] A. Makarovski, A. Zhukov, J. Liu, G. Finkelstein, Phys, Rev. B **75**, 241407(R) (2007).

[18] A. Makarovski, J. Liu, and G. Finkelstein, Phys. Rev. Lett. **99**, 066801 (2007).

[19] K. Grove-Rasmussen, H. I. Jorgensen, and P. E. Lindelof, Physica E **40**, 92 (2007).

[20] F. Kuemmeth, S. Ilani, D. C. Ralph, and P. L. McEuen, Nature **452**, 448 (2008).

[21] T-F. Fang, W. Zuo, and H-G Luo, Phys. Rev. Lett. **101**, 246805 (2008).

[22] F. B. Anders, D. E. Logan, M. R. Galpin, G. Finkelstein, Phys. Rev. Lett. **100**, 086809 (2008).

[23] S. Lipinski, and D. Krychowski, Phys. Rev. B **81**, 115327 (2010).

[24] M. R. Galpin, F. W. Jayatilaka, D. E. Logan, F. B. Anders, Phys. Rev. B **81**, 075437 (2010).

[25] J. P. Cleuziou, N. V. N'Guyen, S. Florens, and W. Wernsdorfer, Phys. Rev. Lett. **111**, 136803 (2013).

[26] S. Sasaki, S. Amaha, N. Asakawa, M. Eto, S. Tarucha, Phys. Rev. Lett. **93**, 017205 (2004).

[27] K. LeHur, and P. Simon, Phys. Rev. B **67**, 201308(R) (2003).

[28] K. LeHur, P. Simon, and D. Loss, Phys. Rev. B **75**, 035332 (2007).

[29] T. Aono, and M. Eto, Phys. Rev. B **63**, 125327 (2001).

[30] M. N. Kiselev, K. Kikoin, and L. W. Molenkamp, Phys. Rev. B **68**, 155323 (2003).

[31] L. Borda, G. Zarand, W. Hofstetter, B. I. Halperin, J. vonDelft, Phys. Rev. Lett. **90**, 026602 (2003).

[32] D. Feinberg, and P. Simon, Appl. Phys. Lett. **85**, 1846 (2004).

[33] A. W. Holleitner, A. Chudnovskiy, D. Pfannkuche, K. Eberl, R. H. Blick, Phys. Rev. B **70**, 075204 (2004).

[34] M. R. Galpin, D. E. Logan, and H. R. Krishnamurthy, Phys. Rev. Lett. **94**, 186406 (2005).

[35] J. Mravlje, A. Ramsak, and T. Rejec, Phys. Rev. B **73**, 241305(R) (2006).

[36] A. Hübel, K. Held, J. Weis, and K. v. Klitzing, Phys. Rev. Lett. **101**, 186804 (2008).

[37] A. M. Chang, and J. C. Chen, Rep. Prog. Phys. **72**, 096501 (2009).

[38] Y. Okazaki, S. Sasaki and K. Muraki, Phys. Rev. B **84**, 161305(R) (2011).

[39] Y. Nishikawa, A. C. Hewson, Daniel J. G. Crow, and J. Bauer, Phys. Rev. B **88**, 245130 (2013).

[40] S. Amasha, A. J. Keller, I. G. Rau, A. Carmi, J. A. Katine, H. Shtrikman, Y. Oreg, and D. Goldhaber-Gordon, Phys. Rev. Lett. **110**, 046604 (2013).

[41] A. J. Keller, S. Amasha, I. Weymann, C. P. Moca, I. G. Rau, J. A. Katine, H. Shtrikman, G. Zaránd, and D. Goldhaber-Gordon, Nature Physics **10**, 145 (2014).

[42] Z-Q. Bao, A-M Guo, and Q-F Sun, J. Phys.: Condens. Matter **26**, 435301 (2014).

[43] M. Filippone, C. P. Moca, G. Zarand, and C. Mora, Phys. Rev. B **90**, 121406(R) (2014).

[44] C. L. Kane and E. J. Mele, Phys. Rev. Lett. **95**, 226801 (2005).

[45] B. A. Bernevig, T. L. Hughes, and S.-C. Zhang, Science **314**, 1757 (2006).

[46] L. Fu, C. L. Kane, and E. J. Mele, Phys. Rev. Lett. **98**, 106803 (2007).

[47] R. Roy, Phys. Rev. B **79**, 195322 (2009).

[48] J. E. Moore, Nature(London) **464**, 194 (2010).

[49] M. König, S. Wiedmann, C. Brüne, A. Roth, H. Buhmann, L. W. Molenkamp, X-L. Qi, S-C. Zhang, Science **318**, 766 (2007).

[50] D. Hsieh, D. Qian, L. Wray, Y. Xia, Y. S. Hor, R. J. Cava, and M. Z. Hasan, Nature (London) **452**, 970 (2008).

[51] D. Hsieh, Y. Xia, D. Qian, L. Wray, J. H. Dil, F. Meier, J. Osterwalder, L. Patthey, J. G. Checkelsky, N. P. Ong, A. V. Fedorov, H. Lin, A. Bansil, D. Grauer, Y. S. Hor, R. J. Cava, and M. Z. Hasan, Nature (London) **460**, 1101 (2009).

[52] Z. Alpichshev, J. G. Analytis, J.-H. Chu, I. R. Fisher, Y. L. Chen, Z. X. Shen, A. Fang, and A. Kapitulnik, Phys. Rev. Lett. **104**, 016401 (2010).

[53] X. Y. Feng, W. Q. Chen, J. H. Gao, Q. H. Wang, F. C. Zhang, Phys. Rev. B **81**, 235411 (2010).

[54] R. Zitko, Phys. Rev. B **81**, 241414(R) (2010).

[55] M-T. Tran, and K-S. Kim, Phys. Rev. B **82**, 155142 (2010).

[56] A. K. Mitchell, D. Schuricht, M. Vojta, L. Fritz, Phys. Rev. B **87**, 075430 (2013).

[57] X. Xin, and M-C. Yeh, J. Phys.: Condens. Matter **25**, 286001 (2013).

[58] I. Kuzmenko, Y. Avishai, and T. K. Ng, Phys. Rev. B **89**, 035125 (2014).

[59] S. Cho, D. Kim, P. Syers, N. P. Butch, J. Paglione, and M. S. Fuhrer, Nano Lett. **12**, 469 (2012).

[60] K. Chang, and W. K. Lou, Phys. Rev. Lett. **106**, 206802 (2011).

[61] D.-H. Lee, Phys. Rev. Lett. **103**, 196804 (2009).

[62] V. Parente, P. Lucignano, P. Vitale, A. Tagliacozzo, F. Guinea, Phys. Rev. B **83**, 075424 (2011).

[63] B. Zhou, H. Z. Lu, R. L. Chu, S. Q. Shen, Q. Niu, Phys. Rev. Lett. **101**, 246807 (2008).

[64] Y. Meir, N. S. Wingreen and P. A. Lee, Phys. Rev. Lett. **66**, 3048 (1991).

[65] C. Lacroix, J. Phys. F **11**, 2389 (1981).

[66] J. R. Schrieffer, and P. A. Wolff, Phys. Rev. **149**, 491 (1966).

[67] M. Eto, J. Phys. Soc. Jpn. **74**, 95 (2005).

[68] R. Lopez, D. Sanchez, M. Lee, M-S. Choi, P. Simon, and K. LeHur, Phys. Rev. B **71**, 115312 (2005).

[69] A. L. Chudnovskiy, Europhys. Lett., **71**(4), 672 (2005).

[70] Y. Meir and N. S. Wingreen, Phys. Rev. Lett. **68**, 2512 (1992).